SAND2017-8374C

Optimal Field Voltage and Energy Storage Control for Stabilizing Synchronous Generators on Flexible AC Transmission Systems

David Rosewater
Sandia National Laboratories
Albuquerque, New Mexico

Quan Nguyen, Surya Santoso
Department of Electrical and Computer Enginnering
University of Texas at Austin

***Abstract*—Power systems can become unstable under transient periods such as short-circuit faults, leading to equipment damage and large scale blackouts. Power system stabilizers (PSS) can be designed to improve the stability of generators by quickly regulating the exciter field voltage to damp the swings of generator rotor angle and speed. The stability achieved through exciter field voltage control can be further improved with a relatively small, fast responding energy storage system (ESS) connected at the terminals of the generator that enables electrical power damping. PSS are designed and studied using a single-machine infinite-bus (SMIB) model. In this paper, we present a comprehensive optimal-control design for a flexible ac synchronous generator PSS using both exciter field voltage and ESS control including estimation of unmeasurable states. The controller is designed to minimize disturbances in rotor frequency and angle, and thereby improve stability. The design process is based on a linear quadratic regulator of the SMIB model with a test system linearized about different operating frequencies in the range 10 Hz to 60 Hz. The optimal performance of the PSS is demonstrated along with the resulting stability improvement.**

I. Introduction

Dynamic response in power systems can become unstable, leading to equipment damage and large scale blackouts. Power system stabilizers (PSS) improve the dynamic response of generators by modulating the exciter field voltage. The exciter field in a generator links the mechanical power of the rotor to the electrical power transmitted and used by the grid. A PSS takes measurements of the system states, including the rotor speed, rotor angle, and field voltage of the generator, and calculates a control signal for the reference field voltage that improves the stability of the generator. PSS implementation allows generators to operate at higher power output, over longer, weaker transmission lines, thereby improving the profitability of the capital investment.

Two strategies are employed in this paper to further improve generator dynamic stability: low-frequency power transmission and energy storage power damping. Low-frequency high-voltage ac (LF-HVac) transmission has recently been proposed as an alternative solution to conventional 60-Hz HVac and the high-voltage direct-current (HVdc) approaches for bulk power transfer. LF-HVac transmission not only retains the ability of using existing ac devices, reliable protection scheme, and multi-terminal structure from the 60-Hz HVac but also provide better voltage regulation and system stability [1]. In addition, LF-HVac approximates the high power transfer capability of HVdc transmission if the operating frequency is sufficiently low [2]. Energy storage systems (ESS) can also be used to improve the performance of PSS and further stabilize the grid. An ESS co-located with a generator enables additional control over the power transferred to the grid and modulating its power can improve the dynamic response of the system [3].

This paper investigates the intersection of both of these strategies, along with modern control for PSS, to evaluate the improvement of system stability when they are employed together. The closed-loop optimal design includes a linear quadratic regulator (LQR) [4] and a reduced order observer to account for the difficulty in measuring states such as the quadrature transient terminal voltage of the generator. The proposed analysis can be extended to multi-machine systems.

In the remainder of this paper, Section II describes the structure of the system under consideration and its state space model. Section III elaborates on the design of the optimal closed-loop controller as well as the reduced-oder observer for the PSS. The simulation result and the discussion about the system responses under various operating parameters are shown in Section IV. Section V completes the paper with a conclusion.

II. System Modeling

In [5] a PSS is designed using a simple model of a single machine oscillating with an infinite bus (SMIB). The PSS, with ESS enhancement, is designed and studied through a modified SMIB model in Fig. 1. This model uses an ideal bus, defined to have constant voltage V_{inf} at angle $0°$, to represent the grid. Connected to this bus, by way of a transmission line, is a generator with scalar terminal voltage V_1 at angle θ. The internal voltage leads the voltage at the infinite bus by the angle δ. For simplicity of designing optimal controllers, generator parameters such as voltage and current are translated from the three-phase sinusoidal abc frame into the synchronously rotating frame with *direct* and *quadrature* components.

D. Rosewater acknowledges funding support from the US DOE OE.

Sandia National Laboratories is a multimission laboratory managed and operated by National Technology and Engineering Solutions of Sandia, LLC, a wholly owned subsidiary of Honeywell International, Inc., for the U.S. Department of Energys National Nuclear Security Administration under contract DE-NA-0003525.

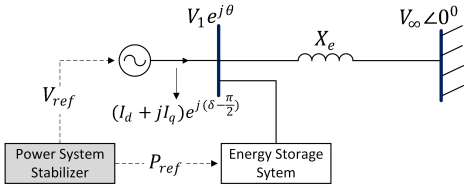

Fig. 1. The model of a single electric machine connected to a infinite bus with PSS and ESS.

The following notation is used throughout this paper:

$\Delta E_q^{'}$	perturbed quadrature-axis transient voltage of the generator,
$\Delta\delta$	perturbed rotor angle,
$\Delta\omega$	normalized perturbed rotor angular velocity;
ΔE_{fd}	d-axis component of the perturbed field voltage in the excitation coil,
ΔP_{ess}	perturbed power supplied (+) or absorbed (-) by the ESS,
K_A	machine amplifier gain,
T_A	machine amplifier time constant,
T_M	mechanical torque applied to the shaft,
$T_{do}^{'}$	direct-axis open-circuit transient time constant of the generator,
V_{ref}	reference steady-state value of terminal voltage,
P_{ref}	reference steady-state value of ESS power,
H	shaft inertia constant of the generator,
D	damping constant of the generator.

A. SMIB Model Equations

The model of SMIB system includes machine differential equations, stator equations, network equations, and ESS equations. In the machine model, the exciter coils generate the magnetic field that enables the spinning rotor to produce electrical voltage on the stator coils. These electromagnetic dynamics are represented in (1). The limits placed on E_{fd} represent safety restrictions on the field voltage and are strictly imposed. The stator equations (2) govern how energy in the rotor is transferred from and to the stator, while the network equations (3) represent the power transfer across the transmission line between the generator and the infinite bus. The first order response dynamics, energy function, and power limits of the ESS are shown in (4). This adaptation of the ESS model from [6] ignores reactive power, auxiliary power, and the dynamic converter model. ESS energy limits are an output of simulation to be used as design requirements for a practical ESS, and charge/discharge power limits are held constant and is strictly imposed in simulation to explore the effect of ESS power saturation on the controller's performance.

Machine equations [5]:

$$\begin{aligned}
\dot{\delta} &= \Delta\omega_{pu}\omega_s, \\
\dot{\omega}_{pu} &= \frac{1}{2H}\left[T_M - (E_q^{'}I_q + (X_d - X_d^{'})I_d I_q + D\Delta\omega_{pu})\right], \\
\dot{E}_q^{'} &= \frac{1}{T_{do}}(-E_q^{'} - (X_d - X_d^{'})I_d + E_{fd}), \\
E_{fd,min} &\le E_{fd} \le E_{fd,max}.
\end{aligned} \tag{1}$$

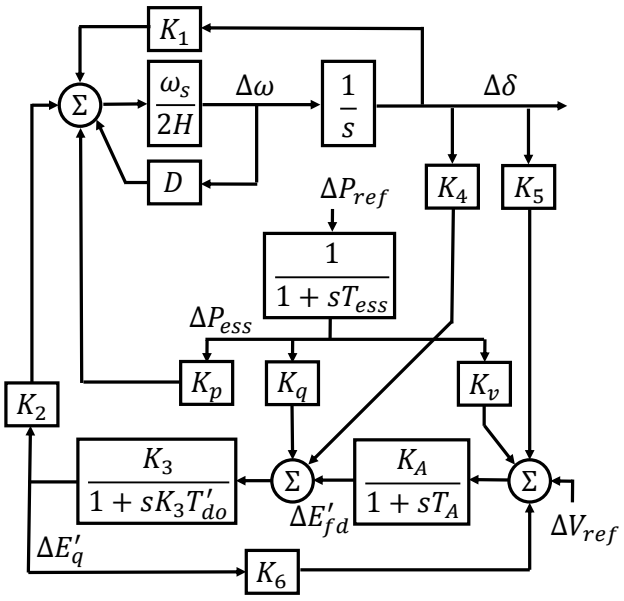

Fig. 2. Block diagram representing the system shown in Fig 1.

Stator equations [5]:

$$\begin{aligned}
X_q I_q - V_d &= 0, \\
E_q^{'} - V_q - X_q^{'} I_q &= 0.
\end{aligned} \tag{2}$$

Network equations [5]:

$$\begin{aligned}
R_e I_d - X_e I_q &= V_d - V_{\inf} sin\delta, \\
X_e I_d + R_e I_q &= V_q - V_{\inf} cos\delta.
\end{aligned} \tag{3}$$

Energy storage equations [6]:

$$\begin{aligned}
P_{ess} &= \frac{P_{ref}}{1 + sT_{ess}}, \\
\dot{E}_{ess} &= P_{ess}, \\
P_{ess,min} &\le P_{ess} \le P_{ess,max}.
\end{aligned} \tag{4}$$

B. State Space Model

Based on (1) - (4), the linearized state-space model of the SMIB is shown in (5) and (6), where K_1-K_6 are given from [5] and new coefficients K_p, K_q, and K_v are given in [3]. The values of these coefficients depends on the reactances X_q, X_d, $X_d^{'}$, and X_e as well as the shaft inertial constant H. While the reactances are each proportional to the operating frequency, H is proportional to the operating frequency squared [5]. The block diagram of the system is shown in Fig. 2, which is the combination of the classical PSS model and the integrated ESS model. Besides the only control input ΔV_{ref} in the classical SMIB model, (5) has another control input ΔP_{ref}, which is the perturbed reference power of the ESS. The saturation limits on the field voltage E_{fd} and ESS power P_{ess} are imposed. The state space output $\mathbf{z}$ is a 4×1 vector that represents the four measurable states. As $\Delta E_q^{'}$ is assumed to be unmeasurable in this design, the first column of the $\mathbf{C}$ matrix is zeros.

$$\begin{bmatrix} \Delta\dot{E}_q^{'} \\ \Delta\dot{\delta} \\ \Delta\dot{\omega} \\ \Delta\dot{E}_{fd} \\ \Delta\dot{P}_{ess} \end{bmatrix} = \begin{bmatrix} -\frac{1}{K_3T_{do}^{'}} & -\frac{K_4}{T_{do}^{'}} & 0 & \frac{1}{T_{do}^{'}} & \frac{K_q}{T_{do}^{'}} \\ 0 & 0 & \omega_s & 0 & 0 \\ -\frac{K_2}{2H} & -\frac{K_1}{2H} & -\frac{D\omega_s}{2H} & 0 & \frac{K_p}{2H} \\ -\frac{K_AK_6}{T_A} & -\frac{K_AK_5}{T_A} & 0 & -\frac{1}{T_A} & -\frac{K_AK_v}{T_A} \\ 0 & 0 & 0 & 0 & -\frac{1}{T_{ess}} \end{bmatrix} \times \begin{bmatrix} \Delta E_q^{'} \\ \Delta\delta \\ \Delta\omega \\ \Delta E_{fd} \\ \Delta P_{ess} \end{bmatrix} + \begin{bmatrix} 0 & 0 \\ 0 & 0 \\ 0 & 0 \\ \frac{K_A}{T_A} & 0 \\ 0 & \frac{1}{T_{ess}} \end{bmatrix} \begin{bmatrix} \Delta V_{ref} \\ \Delta P_{ref} \end{bmatrix}, \quad (5)$$

$$\mathbf{z} = \mathbf{C}\mathbf{x} = \begin{bmatrix} 0 & 1 & 0 & 0 & 0 \\ 0 & 0 & 1 & 0 & 0 \\ 0 & 0 & 0 & 1 & 0 \\ 0 & 0 & 0 & 0 & 1 \end{bmatrix} \begin{bmatrix} \Delta E_q^{'} \\ \Delta\delta \\ \Delta\omega \\ \Delta E_{fd} \\ \Delta P_{ess} \end{bmatrix}. \quad (6)$$

III. Optimal Controller Design

A. The LQR Optimal Controller

A closed-loop controller is designed to improve the stability of the SMIB systems by changing the eigenvalues of the open-loop system to desired values. This controller is designed to minimize a performance index, which is chosen based on the specific requirements of the system and its application. In this paper, the performance index in (7) is defined to minimize the disturbances in rotor frequency $\Delta\omega$ or angle $\Delta\delta$ as well as the control inputs ΔV_{ref} and ΔP_{ref}:

$$L = \frac{1}{2}\int_0^\infty \left[(\Delta\delta)^2 + (\Delta\omega)^2 + r_1(\Delta V_{ref})^2 + r_2(\Delta P_{ref})^2\right]dt \quad (7)$$

Positive definite weights r_1 and r_2 are applied to the input variables which enable adjustment of their relative and absolute utilization by the controller. The optimal control $\mathbf{u}^*$ which minimizes (7) is determined as follows [4]:

$$\mathbf{u}^* = -\mathbf{K}\mathbf{x}, \quad \mathbf{K} = \mathbf{R}^{-1}\mathbf{B}^T\mathbf{S}^*, \quad (8)$$

where:

$$\mathbf{R} = \begin{bmatrix} r_1 & 0 \\ 0 & r_2 \end{bmatrix}, \quad (9)$$

and $\mathbf{S}^*$ is the steady-state solution of the matrix Ricattii equation, which is defined as follows [4]:

$$\dot{\mathbf{S}} = -\mathbf{S}\mathbf{A} - \mathbf{A}^T\mathbf{S} - \mathbf{Q} + \mathbf{S}\mathbf{B}\mathbf{R}^{-1}\mathbf{B}^T\mathbf{S} = \mathbf{0}. \quad (10)$$

With this optimal control, the closed-loop eigenvalues are calculated as follows:

$$|\lambda\mathbf{I} - (\mathbf{A} - \mathbf{B}\mathbf{K})| = \mathbf{0}. \quad (11)$$

B. Reduced Order Observer Design

In practice, measuring the quadrature transient terminal voltage of the generator is not trivial. Therefore, in this design, it is assumed that $\Delta E_q^{'}$ is unmeasurable in that there is no sensor that is able to feed data to a controller. Therefore, $\Delta E_q^{'}$ needs to be estimated based on the measurements of the other states along with the system state equations in (5) and (6). A reduced order observer used to estimate the value of $\Delta E_q^{'}$ is designed as follows. Let the observer $\varphi = \Delta E_q^{'}$ be a linear combination of system states that is unmeasurable and independent of the measurements $\mathbf{z}$:

$$\varphi = \mathbf{T}\mathbf{x} \Rightarrow \dot{\varphi} = \mathbf{T}\dot{\mathbf{x}} = \mathbf{T}\mathbf{A}\mathbf{x} + \mathbf{T}\mathbf{B}\mathbf{u} \quad (12)$$

where $\mathbf{T} = [t_1\ t_2\ t_3\ t_4\ t_5]$ is unknown and $[\mathbf{T}\ \mathbf{C}]^T$ is nonsingular. From (6) and (12), the system states can be determined as follows:

$$\mathbf{x} = \begin{bmatrix} \mathbf{T} \\ \mathbf{C} \end{bmatrix}^{-1} \begin{bmatrix} \varphi \\ \mathbf{z} \end{bmatrix} = \begin{bmatrix} \mathbf{S}_1\ \mathbf{S}_2 \end{bmatrix} \begin{bmatrix} \varphi \\ \mathbf{z} \end{bmatrix} = \mathbf{S}_1\varphi + \mathbf{S}_2\mathbf{z}. \quad (13)$$

Substituting (13) into (12) yields:

$$\dot{\varphi} = \mathbf{T}\dot{\mathbf{x}} = \mathbf{T}\mathbf{A}\mathbf{S}_1\varphi + \mathbf{T}\mathbf{A}\mathbf{S}_2\mathbf{z} + \mathbf{T}\mathbf{B}\mathbf{u} \quad (14)$$

Let $\hat{\varphi}$ and $\hat{\mathbf{x}}$ are the estimated values of φ and the system states. From (13) and (14), their estimation errors $\tilde{\varphi}$ and $\tilde{\mathbf{x}}$ satisfy the following equations:

$$\dot{\tilde{\varphi}} = \dot{\varphi} - \dot{\hat{\varphi}} = \mathbf{T}\mathbf{A}\mathbf{S}_1(\varphi - \hat{\varphi}) = \mathbf{T}\mathbf{A}\mathbf{S}_1\tilde{\varphi}, \quad (15)$$

and:

$$\dot{\tilde{\mathbf{x}}} = \mathbf{S}_1\dot{\varphi} = \mathbf{S}_1\mathbf{T}\mathbf{A}\mathbf{S}_1\tilde{\varphi} = \mathbf{S}_1\mathbf{T}\mathbf{A}\tilde{\mathbf{x}} = (\mathbf{I} - \mathbf{S}_1\mathbf{C})\mathbf{A}\tilde{\mathbf{x}} \quad (16)$$

The coefficient matrix $(\mathbf{I} - \mathbf{S}_1\mathbf{C})\mathbf{A}$ has the following non-zero eigenvalue:

$$\lambda_{obs} = \frac{1}{K_3T_{do}^{'}} - \frac{t_3}{t_1}\frac{K_2}{2H} - \frac{t_4}{t_1}\frac{K_AK_6}{T_A}. \quad (17)$$

In order to guarantee system stability when the observer is implemented, the eigenvalue in (17) is chosen to be much faster than the eigenvalues of the closed-loop system obtained in the previous section.

IV. Simulation Results

This section shows the response of a test system, as shown in Fig. 1, without and with the designed optimal controllers described in Section III. The effect of the operating frequency on the response of the system under disturbances is also included. The remainder of this section addresses the effect of weighting factors in the performance index on the system response.

The parameters of the test system at 60 Hz are $T_{do}^{'}$ = 9.6 sec, K_A = 400, D = 0, X_q = 2.1 p.u, X_d = 2.5 p.u, $X_d^{'}$ = 0.39 p.u, H = 3.2, T_A = 0.2 sec, and T_{ess} = 0.01667 sec, R_e = 0, X_e = 0.5, V_t = 1 p.u, θ_t = 15°, V_∞ = 1.05 p.u, θ_∞ = 0° [5]. These values are consistent with a high-speed water wheel or non-condensing turbine generator with a 100 MVA rating. The state limits are $E_{fd,min}$ = -0.5 p.u, $E_{fd,max}$ = 0.5 p.u, $P_{ess,min}$ = -0.1 p.u, and $P_{ess,max}$ = 0.1 p.u.

A. The Open-Loop System Response

At a frequency of 60 Hz the open-loop eigenvalues of the system without any closed-loop controllers are:

$$\lambda_1 = -60, \lambda_{2,3} = -2.588 \pm j8.502, \lambda_{4,5} = -0.087 \pm j7.114.$$

The eigenvalues of the open-loop system have negative real parts; therefore, the system is stable. However, λ_4 and λ_5 are close zero, which means that the system might become unstable under large disturbances. λ_1 is the eigenvalue of the ESS controller. Table I shows the settling times for the open-loop system from 60 Hz to 10 Hz. Settling time is measured as the time it takes for the states to enter and remain in a 2% error band. Reducing the operating frequency from 60 Hz to 40 Hz results in shorter settling times. Settling time then increases at 30 Hz and becomes unstable below 20 Hz.

TABLE I
OPEN-LOOP SETTLING TIME PERFORMACE

State	60 Hz	50 Hz	40 Hz	30 Hz	20 Hz	10 Hz
$\Delta\delta(sec.)$	63.3655	17.0457	15.8578	35.4401	∞	∞
$\Delta\omega(sec.)$	62.7212	17.2029	15.9886	35.5478	∞	∞

B. The Closed-Loop System Response

The rotor speed is assumed to have a initial disturbance of 0.12 Hz. The weighting factors of the input controls ΔV_{ref} and ΔP_{ref} in (7) are chosen to be $r_1 = 1$ and $r_2 = 0.01$, respectively. With the closed-loop optimal control described in Section III.A, the eigenvalues of the 60 Hz system become:

$$\lambda_1 = -52.428, \lambda_2 = -28.245,$$
$$\lambda_3 = -13.920, \lambda_{4,5} = -4.974 \pm j10.537.$$

Since these eigenvalues are pushed further from the imaginary axis, the stability of the system is improved.

The reduced order observer described in Section III.B is determined by first choosing $t_2 = t_5 = 0$ and $t_3 = t_4 = 1$, and then solving for t_1 using (17). With the eigenvalue of the observer being $\lambda_{obs} = -300$, the performance of the observer when the operating frequency is 60 Hz is shown in Fig. 3. The initial error between the actual and estimated values of the quadrature transient terminal voltage of the generator becomes zero shortly after 0.1 seconds.

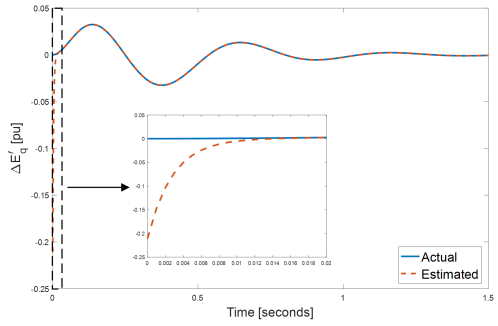

Fig. 3. Observer performance.

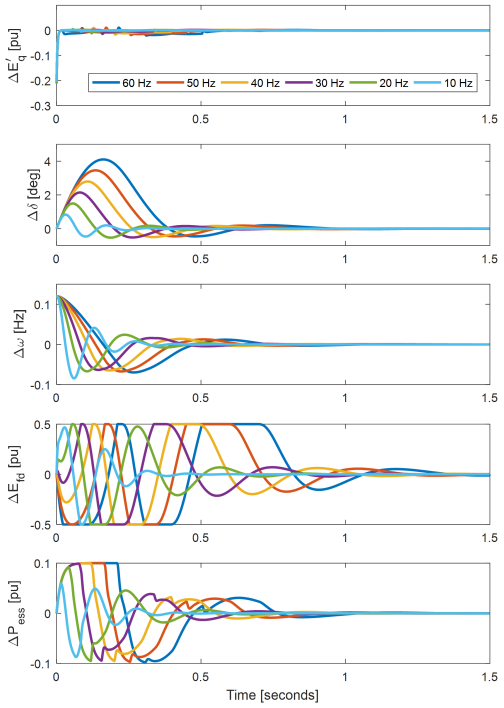

Fig. 4. The response of states at each frequency of interest.

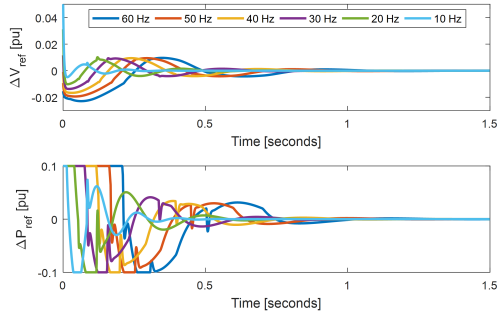

Fig. 5. Optimal controls.

TABLE II
CLOSED-LOOP SETTLING TIME PERFORMACE

State	60 Hz	50 Hz	40 Hz	30 Hz	20 Hz	10 Hz
$\Delta\delta(sec.)$	0.8755	0.7724	0.6608	0.6490	0.5130	0.3395
$\Delta\omega(sec.)$	0.9214	0.8188	0.7095	0.5875	0.5371	0.3581

With the designed reduced order observer, the response of the states and the optimal input controls to the initial rotor speed disturbance of 0.12 Hz at different operating frequencies is shown in Fig. 4. The optimal control is shown in Fig. 5, where a lower input control is needed at a lower frequency. Table II shows the improved settling time response of the rotor speed and angles. Compared to the open-loop response, the closed-loop controller improves the settling time by more than a factor of 60 at 60 Hz. It is also able to stabilize the system at operating frequencies lower than 20 Hz while continuing to

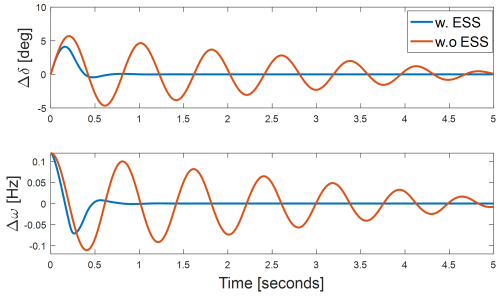

Fig. 6. Energy Storage Response

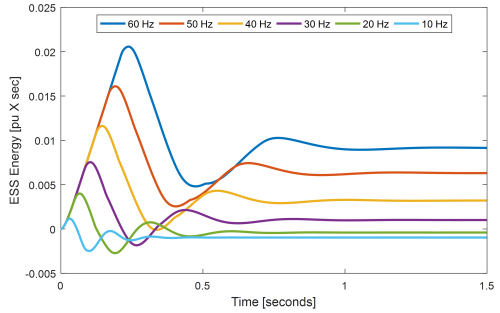

Fig. 7. Energy Storage Response

improve the settling time.

Fig. 6 shows the response of states to the initial rotor speed disturbance with and without the use of ESS. The ESS helps to quickly stabilize the system after 0.5 second, compared to more than 5 seconds when the EES is not deployed. Fig. 7 shows the result of energy required from the ESS at different operating frequencies to suppress the initial rotor speed disturbance. At 60 Hz, the ESS has a peak change in energy of 0.0119 p.u power seconds. This would mean that a 100 MVA generator at 60 Hz would require 1.19 MWs (19.8 kWh) of energy supplied/absorbed from storage to achieve this performance. Lower frequencies require less energy reserves to supply the desired damping. The same generator operating at 10 Hz would only require 230 kWs (3.83 kWh) of energy to achieve this performance.

C. The Effect of Weighting Factors in the Performance Index

This section shows the effects of adjusting the input weighting factors in the LQR performance index (7). Fig. 8 shows the response of rotor speed and angle when the weighting factor r_2 of ΔP_{ess} increases from 0.01 as in the previous studies to 0.5, and then to ∞. The coefficients of the other components are kept constant, and the operating frequency is 60 Hz. Practically, this allows designers to adjust the requirements of the energy storage system to reach a stability performance target. Reducing r_2 results in a higher deployment the ESS, which improves the stability performance of the system. Table III shows the settling time as r_2 in (7). When compared to the case where energy storage is not used $r_2 = \infty$, settling time is more than cut in half when $r_2 = 0.5$ and halved again when $r_2 = 0.01$.

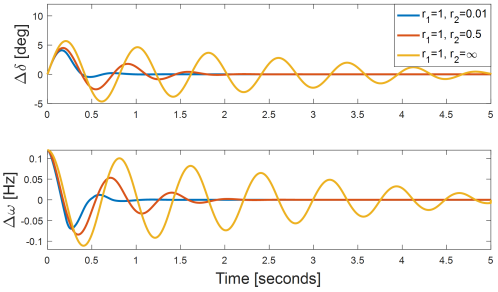

Fig. 8. The resulting states when r_2 varies.

TABLE III
SETTLING TIME PERFORMANCE WITH REDUCED ESS CONTROL ACTION

State	$\mathbf{r_2 = 0.01}$	$\mathbf{r_2 = 0.5}$	$\mathbf{r_2 = \infty}$
$\Delta\delta(sec.)$	0.8755	1.9639	5.2233
$\Delta\omega(sec.)$	0.9214	1.8569	5.3269

V. Conclusion

An optimal closed-loop controller is designed for PSS to improve the stability of a generator using both the reference field voltage and ESS power as input controls. This controller minimizes the perturbations in rotor frequency and angle in response to disturbances. The designed reduced order observer is able to exactly estimate the unmeasurable state after 0.1 seconds. At 60 Hz and with the same initial rotor speed disturbance of 0.12 Hz, the open loop-system requires 63 seconds to settle, while the proposed controller reduces the settling time to 5.3 seconds without the use of ESS and 0.92 second with the ESS. At a lower operating frequency of 10 Hz, the open-loop system is unstable while the closed-loop system is stable and has a settling time of 0.34 second. With the proposed closed-loop controller the ESS requires less energy to be effective at low frequencies. To damp out the same disturbance, the system operating at 10 Hz only needs 3.83 kWh of energy, while 19.8 kWh is required when the operating frequency is 60 Hz.

References

[1] T. Funaki and K. Matsuura, *"Feasibility of the low frequency AC transmission,"* IEEE Power Engineering Society Winter Meeting, 2000.
[2] T. Ngo and M. Lwin and S. Santoso, *"Steady-State Analysis and Performance of Low Frequency AC Transmission Lines,"* IEEE Transactions on Power Systems, vol. PP, no. 99, pp. 18, 2015.
[3] C. Zhongwei et al *"Application of flywheel energy storage to damp power system oscillations,"* Przeglad Elektrotechniczny (Electrical Review), 2011.
[4] F. L. Lewis, and D. Vrabie, and V. L. Syrmos, *"Optimal Control,"* 3rd Edition, Wiley, 2012.
[5] P. Sauer and M. Pai, *"Power system dynamics and stability,"* Prentice Hall, Potsdam, 1998.
[6] P. Pourbeik *"WECC Energy Storage System ModelPhase II,"* WECC Renewable Energy Modeling Task Force, 2015.